Current Chemistry Letters 12 (2023) 799–812

Contents lists available at GrowingScience

Current Chemistry Letters

homepage: www.GrowingScience.com

Green synthesis, characterization, and biological activities of Zn, Cu monometallic and bimetallic nanoparticles using *Borassus flabellifer* leaves extract

Supriya Dubey[a], Abha Shukla[a*] and Rishi Kumar Shukla[b]

[a]*Department of Chemistry, KGC, Gurukula Kangri (Deemed to be University), Haridwar, India- 249407*
[b]*Department of Chemistry, Gurukula Kangri (Deemed to be University), Haridwar, India- 249404*

C H R O N I C L E

Article history:
Received December 25, 2022
Received in revised form
January 28, 2023
Accepted April 19, 2023
Available online
April 19, 2023

Keywords:
Green synthesis
Borassus flabellifer
Bimetallic oxide nanoparticles
Zinc
Copper

A B S T R A C T

In the present work, Zn, Cu monometallic and bimetallic nanoparticles were synthesized using leaves extract of *Borassus flabellifer*. Plant extract acts as both surfactant and reducing agent. The synthesized nanoparticles were characterised by UV-Vis, XRD, FESEM, EDX, and HRTEM techniques. UV-Vis spectroscopy is used to monitor the synthesis of nanoparticles. XRD technique was used to confirm the amorphous nature of nanoparticles. The FESEM images demonstrate that the shape of the nanoparticles such as Zn monometallic (pseudo-spherical), Cu monometallic (rod), Zn-Cu bimetallic are (pseudo-spherical and rod-shaped). HRTEM images show the approximate size of the Zn, Cu monometallic and Zn-Cu bimetallic nanoparticles is 3.0 nm, 3.52 nm and 2.2 nm respectively. EDX spectra confirm the presence of Zn, Cu and O in the sample. Synthesized Zn, Cu monometallic nanoparticles, and Zn-Cu bimetallic nanoparticles were used to evaluate their possible antimicrobial, antidiabetic and antioxidant properties. Bimetallic nanoparticles displayed higher antioxidant, antidiabetic, and antimicrobial properties in the comparison of monometallic nanoparticles. The results suggest that Zn-Cu bimetallic nanoparticles have greater potential than monometallic nanoparticles.

1. Introduction

Nanotechnology is a rapidly expanding field in which research is focused on the synthesis, design, and manipulation of particle structures[1]. Nanoparticles (NPs) have a wide range of uses in the chemical, pharmaceutical, food, medical, optical, and other sectors in the treatment of diseases[2]. The unique properties displayed by the nanoparticles are due to the increase in surface to volume ratio which alters the catalytic properties of nanoparticles[3]. Moreover, metal nanoparticles are well acknowledged to possess anticancer, antioxidant, antibacterial properties and to play a significant role in wound healing[4]. It is interesting to mention that nanoparticles have many different applications in organic and applied chemistry[5-7]. Nanoparticle synthesis by chemical and physical methods is expensive and produces harmful by products in the environment[8]. Due to these problems, it is necessary to use a bio-green approach for the synthesis of nanoparticles using microorganisms or extracts of medicinal plants, which has received a lot of attention from researchers[9]. Green synthesis methods are becoming more and more popular because of the low cost and environment- friendly synthesis of nanoparticles. There are many instances of green, natural, and environmentally friendly reducing and capping agents being used in the production of nanomaterials. Some parts of plants such as leaves, fruits, roots, stem, seeds have been used for the synthesis of various nanoparticles because the extract contains phytochemicals that serve as stabilising and reducing agents. Nanoparticles synthesized from many medicinal plants such as Agathosma betulina[10], Plumbago auriculata[11], Monsomia burkeana[12], Lessertia montana[13], Lessertia frutescens[14], Tulbaghia violacea[15], Aspalathus linearis[16], Dovyalis caffra[17], Athrixia phylicoides[18]. The extract contains phytochemicals (alkaloids, amino acids, ascorbic acid, oxalic acid, carboxylic

* Corresponding author. Tel.: +9219855406
E-mail address abha.shukla@gkv.ac.in (A. Shukla)

doi: 10.5267/j.ccl.2023.4.002

acid, polyphenols, flavoniods, alcohols, terpeniods, glycosides, carbohydrates, thiamin, vitamin C, and polyols) that reduce and stabilise the NPs[19].

Transition metals have been widely used in different fields like in catalyst [20-24] as well as in synthesis of nanoparticles[19]. Zinc is a crucial trace element that is widely distributed across all body tissue. Zinc is a key element in many enzyme systems and is essential for the production of proteins and nucleic acids[25]. It also plays an important role in hematopoiesis and neurogenesis. ZnO nanoparticles have excellent antimicrobial and UV-blocking properties. Zinc oxide (ZnO) has the confirmed biocompatibility summary that "generally recognised as safe" (GRAS) material to the human and animal system by the USFDA (21CFR182.8991) and plays a dynamic role in the day-to-day life of the third uppermost universal making volume only after SiO2 and TiO2 among the safest metals to use[26]. Due to their high photocatalytic degradation, ZnONPs are utilised in textiles for water treatment and sunscreen.

Copper is an essential trace metal element in the human body which is primarily absorbed in the stomach and small intestine and excreted in the bile[27]. It has special abilities to protect the cardiovascular system, accelerate bone fracture repair, and have antimicrobial effects. Moreover, copper can be utilised in radiotherapy for cancer, Positron Emission Tomography (PET) imaging, increasing the healing of incisional wounds, and eliminating cancer cells[28]. Copper oxide nanoparticles have grown significantly because of their special qualities and wide range of uses, such as in solar cells, gas sensors, hydrogen storage materials, and medical applications. Therefore, there is a need for biological alternatives of producing ecofriendly NPs[29].

The medicinal plant Palmyra palm with the scientific name of *Borassus flabellifer* from the Arecaceae family was collected from the Northern Indian state of Uttar Pradesh. This plant contains different types of secondary metabolites including glycosidic compounds, fatty acids, terpenoids, phenolics, tannins, anthocyanins, etc. In traditional medicine, *Borassus flabellifer* was utilized to treat wound healing, diabetes, chronic disease etc[30].

From a scientific and technological point of view bimetallic nanoparticles, which combine two different metals, have generated more interest than monometallic nanoparticles[31]. Bimetallic nanoparticles promote the development of new chemical properties than their parent monometallic nanoparticles. From the literature survey, it has been examined that some research articles reported about Zn-Cu bimetallic nanoparticles by green synthesis. But there is no research article reported yet about synthesis of Zn, Cu monometallic and bimetallic NPs using Borassus flabellifer leaves.

In this study Zn, Cu monometallic and bimetallic NPs have been synthesized using *Borassus flabellifer* leaves extract via a green method. The synthesized bimetallic NPs have been characterized by X-ray diffraction (XRD), field emission gun scanning electron microscopy (FEG-SEM), and high resolution transmission electron microscopy (HR-TEM) combined with energy dispersive analysis of X-rays (EDX). Additionally, the antioxidant, antidiabetic and antimicrobial activity of these NPs have been evaluated.

2. Results and discussion

2.1. Ultra violet- visible spectroscopy

UV-VIS spectroscopy is an essential initial tool for gathering data on the emergence of metal NPs in aqueous solutions. Optical absorption spectroscopy has demonstrated that Borassus flabellifer leaves extract can induce the synthesis of ZnO monometallic, CuO monometallic, and Zn-CuO bimetallic nanoparticles. The UV-visible spectra of Zn, Cu MNPs and Zn-Cu BMNPs are represented in **Fig. 1**. From figure 1(a) it has been examined that the peak of Zn monometals precursor at about 230 nm shifts to 365nm and get stable. Shifting of this peak representing the formation of Zn MNPs. Similarly in case of Cu [figure 1(b)] shifting of peaks from 200 nm to 275nm represent the formation of Cu MNPs. The color of the solution changes from sky blue to brown. Change in the color of the solution also represents the reduction of metal ions and formation of new species. It is expected that two absorption peaks are formed for the merger of the Zn and Cu MNPs but the existence of only one new characteristic peak in figure 1(c) shifting from (200nm to 380nm) indicates the formation of Zn-Cu BMNPs. The color of the solution changes from light brown to dark brown also verifies the formation of BMNPs.

2.2. X ray diffraction analysis

The XRD patterns of Zn, Cu, MNPs and Zn-Cu BMNPs are shown in **Fig. 2 (a-c).** The hexagonal phase and crystalline structure of zinc oxide NPs were confirmed by the significant peaks seen in $2\theta = 31.98, 34.81, 36.53, 47.5$ in **Fig. 2.** (JCPDS card 36-1451). The monoclinic copper oxide phases crystal structure was confirmed by the peaks in the $2\theta = 36.58, 38.20, 43.45, 52.47$, and $74.43°$. (JCPDS card 01-080-1917) **(Fig. 2 (b)). Fig. 2** displays the Zn-CuO sample X-ray pattern together with its indexing. The Zn-CuO X-ray pattern peaks perfectly match those of the Zn and CuO samples (found on JCPDS cards with the numbers 36-1451 and 01-080-1917, respectively), confirming the existence of Zn and Cu in the oxide form in the sample. All samples crystallite sizes (Dc) were determined using the Debye-Scherrer formula:

$$Dc = \frac{k\lambda}{\beta Cos\,\theta}$$

where k is shape factor, λ is the radiation wavelength, β is the full width of the observed diffraction peak, Dc is average crystalline size and Zn, Cu, MNPs and Zn-Cu BMNPs samples computed crystallite sizes are 35.84 nm, 38.76 nm, and 7 nm, respectively. Due to the lattice interaction between the zinc and copper content in the bimetallic NPs, it can be seen from the crystallite size values that the Zn-Cu BMNPs sample crystallite size is less than that of the ZnO and CuO sample.

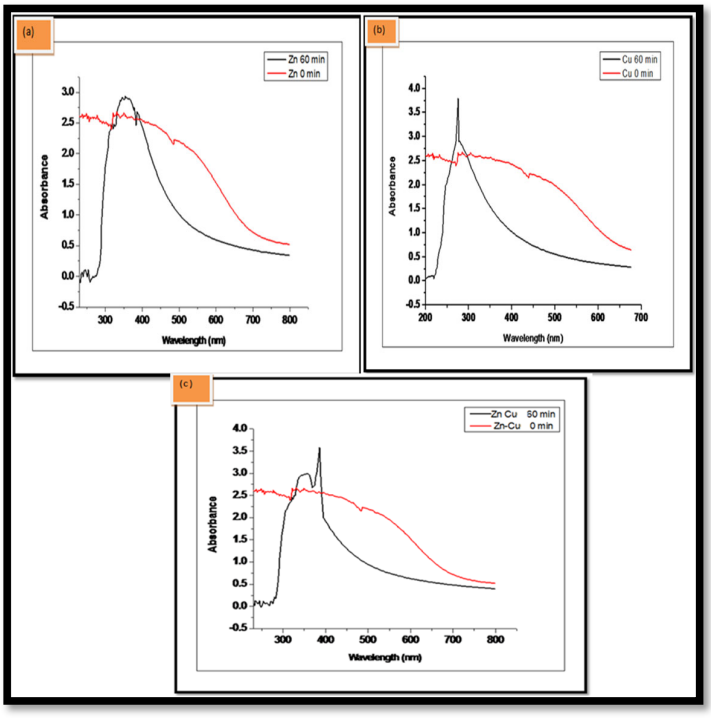

Fig. 1. UV-visible spectra of *Borassus Flabellifer* mediated (a) Zn MNPs (b) Cu MNPs and (c) Zn-Cu BMNPs.

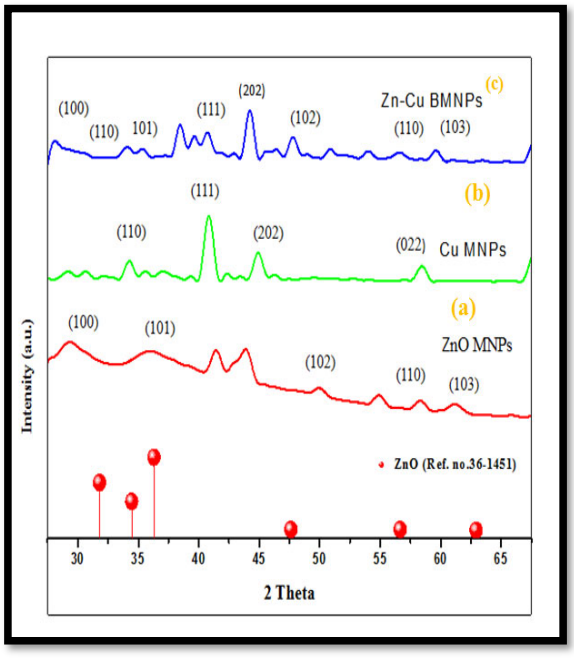

Fig. 2. The XRD pattern of *Borassus flabellifer* leaves extract mediated (a) Zn MMNPs, (b) Cu MMNPs (c) Zn-Cu BMNPs

2.3. FESEM and EDX analysis

The FE-SEM technique has been used to determine the surface morphology of the produced nanopartical samples. FESEM, EDX are shown in **Fig. 3. Fig. 3(a)** represents the pseudo-spherical like (elongated) shape of Borassus flabellifer Zn MNPs. It can be seen from **Fig. 3(c)** that Cu MNPs are rod in shape**. Fig. 3(e)** shows that Zn-Cu BMNPs pseudo-spherical and rod shapes are irregular in shape with some agglomeration. EDX analytical technique are given in **Fig. 3(b), 3(d), 3(f)** respectively. The elemental composition percentage ration of Cu –Zn are 98.83: 1.16. As a result, the atomic composition analysis using EDX shows that the final particles have a core shell structure with Zn in the core and Cu shell.

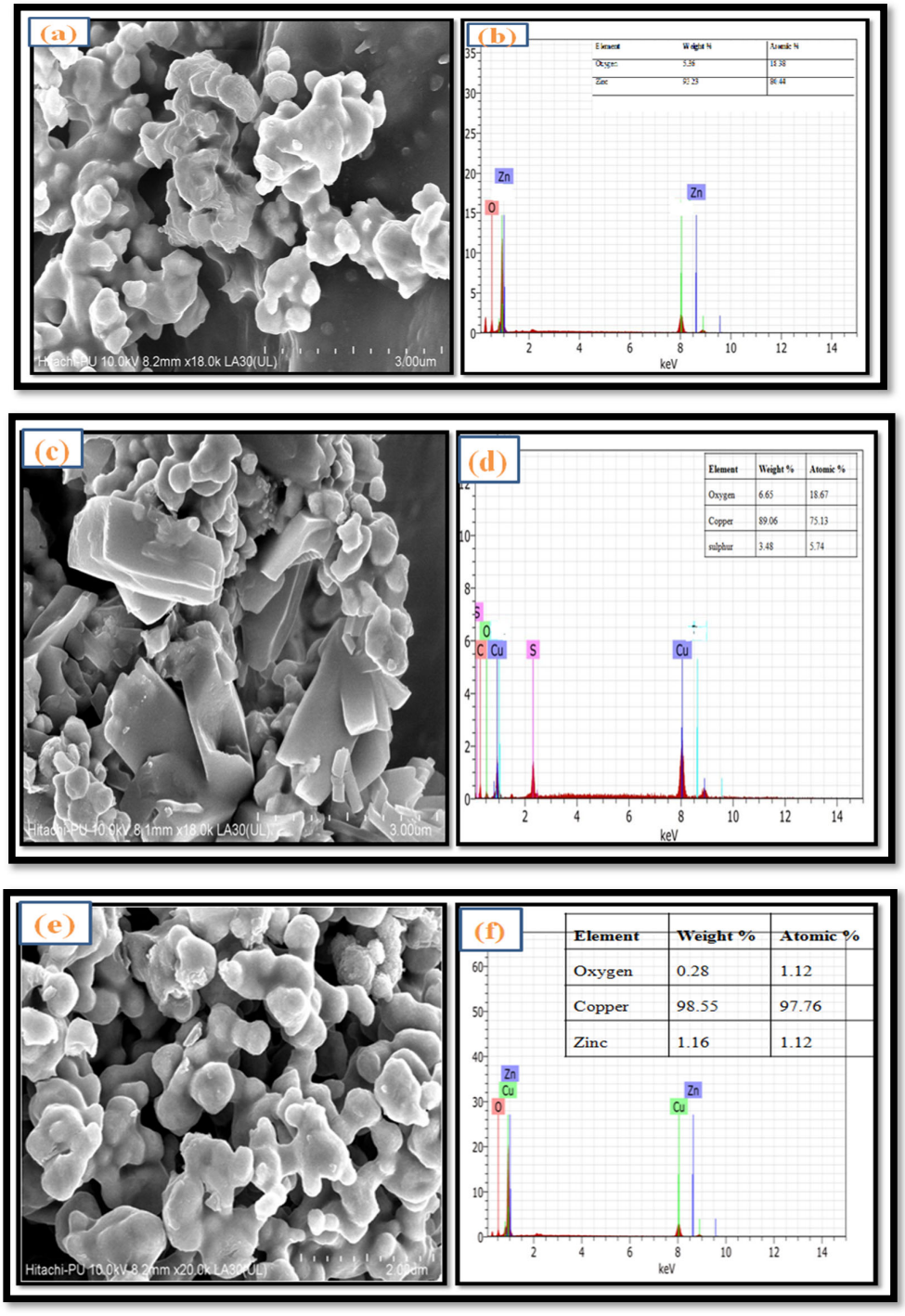

Fig. 3. FESEM, EDX of *Borassus flabellifer* mediated (a-b) Zn, (c-d) Cu, and (e-f) Zn-Cu nanoparticles.

2.4. HR-TEM analysis

HRTEM is the most unusual method for examining the internal structure and size of nanomaterials. The HR-TEM images shown in **Fig. 4 (a, b and c)** were used to examine the morphology and crystallite distribution of Zn, Cu MNPs and Zn-Cu BMNPs mediated by Borassus flabellifer leaves. The histogram 4(i-iii) are evaluated from the corresponding HRTEM images to calculate average particle size of nanocatalysts. The calculated particle size of Zn, Cu mono in image 4(i)-4(ii) is 3.0nm, 3.52nm and for Zn-Cu BMNPs in image 4(iii) is 2.2nm respectively. No agglomeration and uniform distribution of Zn, Cu MNPs and Zn-Cu BMNPs were detected from the HRTEM images.

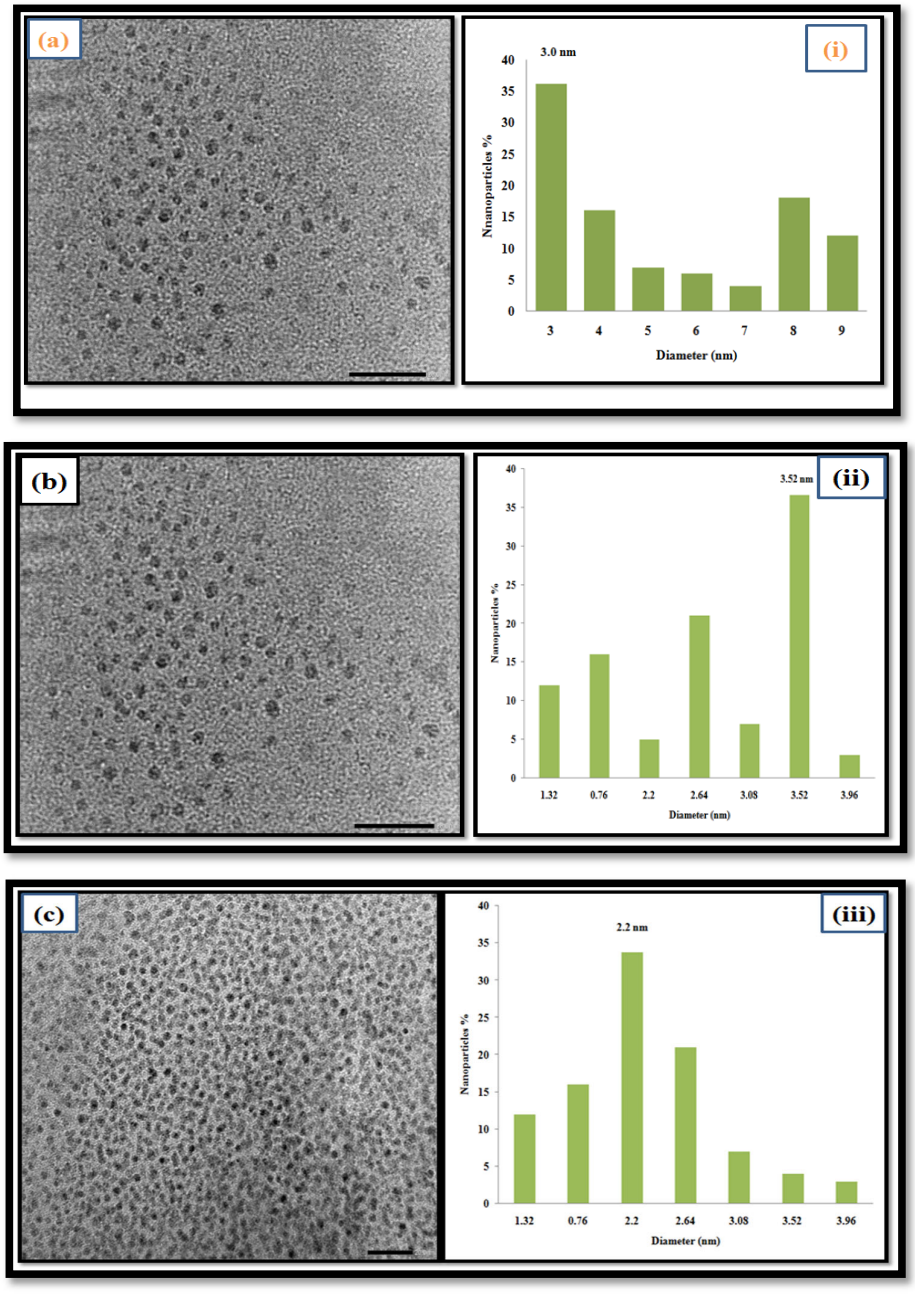

Fig. 4. HRTEM images of *Borassus flabellifer* mediated (a) Zn MNPs (b) Cu MNPs and (c) Zn-Cu BMNPs.

2.5. Total Phenolic and Flavonoid Content

The reaction mixture for phenolics and flavonoids caused various behaviours in the Zn, Cu MNPs, and Zn-Cu BMNPs. Zn, Cu MNPs are significantly less active than BMNPs. Different functional groups on the surfaces of nanoparticles are most likely responsible for these actions. These actions may also be facilitated by zinc and copper ions released from the

NPs. The results of a calibration curve (y = 0.010x+0.483, R2 = 0.999), mg of GA/g of dry sample, were used to determine the total phenolic content. Zn, Cu, MNPs and Zn-Cu BMNPs had total phenolic values of 16.5 ± 0.23, 21.4 ± 0.65, 28 ± 0.91 mg of GA/g of dry sample, respectively. The results of the calibration curve (y = 0.008x + 0.826, R2 = 0.997), mg of quercetin/g of dry material, were used to determine the total flavonoid concentration. Zn, Cu MNPs and Zn-Cu BMNPs have total flavonoid concentrations of 13.75 ± 0.38, 20.37 ± 0.47, 49.25 ± 0.62 mg of quercetin / g of dry sample respectively.

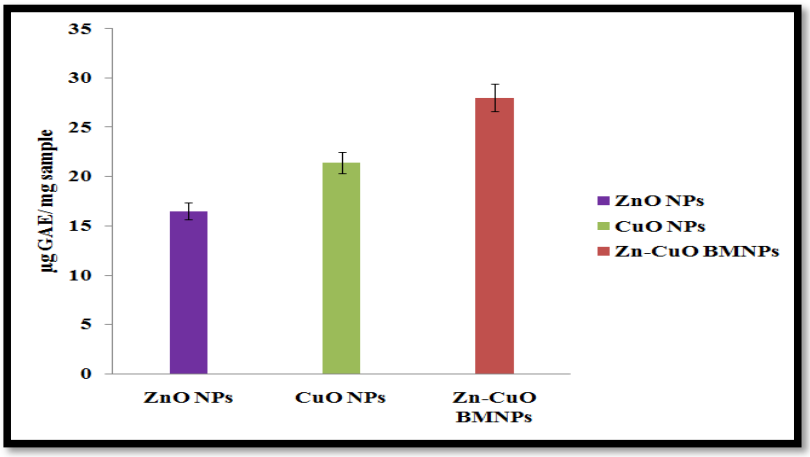

Fig. 5. (a) Total Phenolic Content of Zn, Cu MNPs and Zn- Cu BMNPs

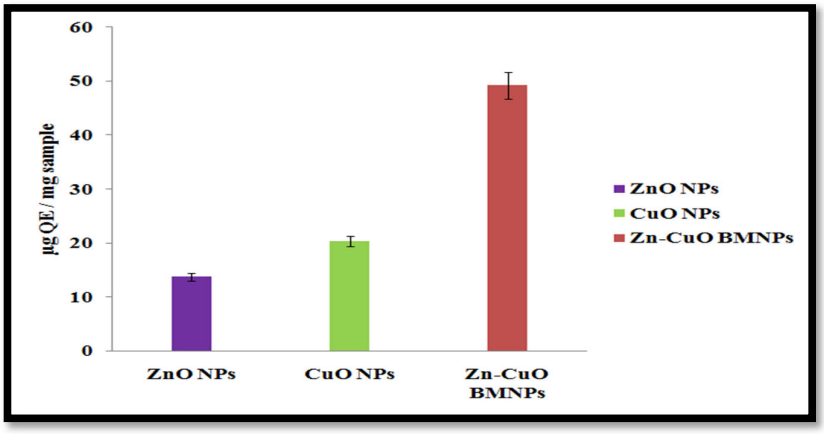

Fig. 5. (b). Total Flavonoid Content of Zn, Cu MNPs and Zn-Cu BMNPs

Table 1. Total Phenolic and Flavonoid Content

Polyphenols	Zn MNPs	Cu MNPs	Zn-Cu BMNPs
Phenolics (mgGAE.gm-1dw)	16.5	21.4	28
Flavonoid (mg quercetin equivalent/g extract)	13.75	20.37	49.25

2.6. Antioxidant Activity

The DPPH reagent discolouration was used to gauge the nanoparticles percentage free radical scavenging activity. The process depends on reducing DPPH (purple in colour) into stable diphenyl picrylhydrazine molecules (yellow in colour) by taking an electron or hydrogen radical from the donor antioxidant. The graphic demonstrates that the activity of free radicals varies slightly. While Zn,Cu MNPs are both capable of scavenging free radicals, Zn-Cu BMNPs are more effective at doing so. Zn, Cu MNPs and Zn-Cu BMNPs had IC_{50} values of 586.94, 342.75, 68.28µg/mL respectively **(Fig. 6 (a)).**

The phosphate/Mo (V) complex, which is green in colour and has a maximum absorption at 695 nm, is generated as a result of the tatal's antioxidant capacity's dependence on the reduction of Mo (VI) to (V) via antioxidant mediators. In comparison to Zn, Cu MNPs, Zn- Cu BMNPs have a higher capacity. Zn, Cu MNPs and Zn-Cu BMNPs had IC_{50} values of 545.59, 311.88, 60.8µg/mL respectively **(Fig. 6 (b)).**

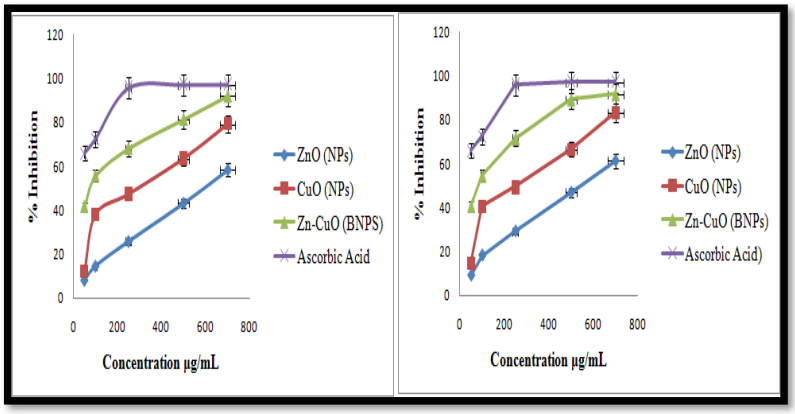

Fig. 6. (a) Free radical scavenging activity (b) Total antioxidant capacity of Zn, Cu MNPs and Zn-Cu BMNPs

Table 2. Free radical scavenging activity of ZnO, CuO MNPs and Zn- CuO BMNPs

S.N.	Samples	IC50µg/ml(DPPH)	IC50µg/ml(Phosphomolybdenum)
1	Zn MNPs	586.94	545.59
2	Cu MNPs	342.75	311.88
3	Zn-Cu BMNPs	68.28	60.8

2.7. Antidiabetic Activity

Inhibition of alpha amylase and alpha glucosidase by Zn, Cu MNPs and Zn-Cu BMNPs

The digestive enzymes for carbohydrates, such as intestinal alpha glucosidase and pancreatic alpha amylase, are labile and can break down oligosaccharides and disaccharides into monosaccharides that are suitable for absorption. Because it will delay the release of glucose into the blood, inhibiting these two digestive enzymes is highly helpful for treating non-insuline diabetes. According to the findings, alpha amylase and alpha glucosidase were strongly suppressed after being incubated with different concentrations of Zn,Cu monometallic, and Zn- Cu BMNPs, as shown in fig. The IC_{50} values of alpha amylase for Zn, Cu MNPs, and Zn-Cu BMNPs were 544.35, 224.04, and 74.54 µg/mL, respectively, and for alpha glucosidase were 545.46, 245.58, and 83.80 µg/mL, as shown in **(Fig. 7 (a) and (b))** Table 3.

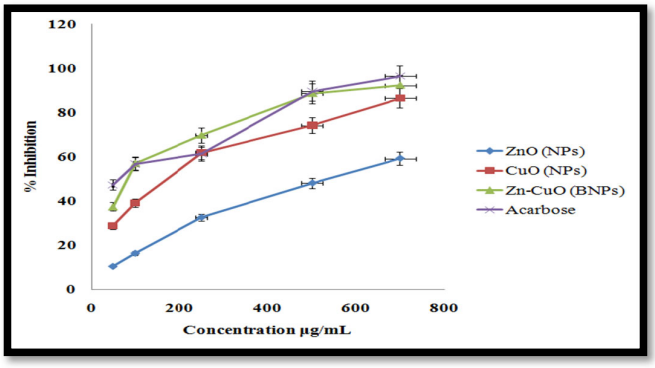

Fig. 7.(a). In vitro effect of Zn, Cu MNPs and Zn-Cu BMNPs on Alpha - amylase

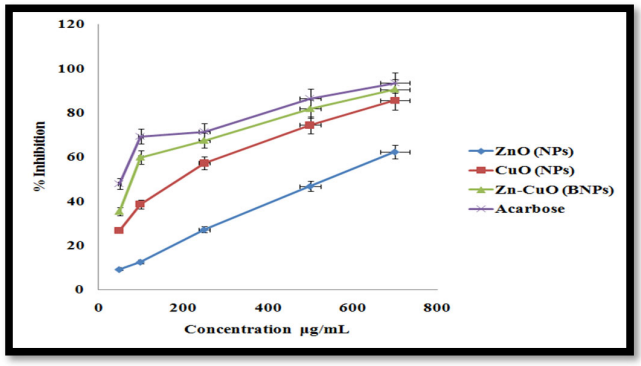

Fig. 7(b). In vitro effect of Zn, Cu MNPs and Zn-Cu BMNPs on Alpha –glucosidase

Table 3. In vitro effect of ZnO and CuO MNPs and Zn- CuO BMNPs on Alpha- amylase and glucosidase

Samples	Antidiabetic activity IC_{50} (µg/ml)	
	α-amylase assay	α-glucosidase assay
ZnO MNPs	544.35	545.46
CuO MNPs	224.04	245.58
Zn- CuO BMNPs	74.54	83.80
Acarbose	59.81	59.81

2.8. Antibacterial Activity

Using the well diffusion method, the antibacterial activity of Borassus flabellifer leaves extract-assisted nanocatalysts was examined against pathogenic bacterial strains of gram-negative Escherichia coli (E. coli), pseudomonas aeruginosa, and gram-positive Staphylococcus aureus **(Fig. 8 a,b,c)**. The antibacterial activity data show that Zn-Cu BMNPs were more effective antibacterials than their Zn, Cu MNPs. Zn-Cu BMNPs produced the largest zone of inhibition against gram-negative E. coli with a diameter of 25 mm, gram-negative pseudomonas aeruginosa with a zone of inhibition of 12 mm, and gram-positive staphylococcus aureus with a zone of inhibition of 11 mm. In contrast to gram-positive staphylococcus aureus and gram-negative pseudomonas aeruginosa, Zn MMNPs produce a 12 mm zone of inhibition against gram-negative E. coli and 11 mm zone of inhibition against pseudomonas aeruginosa, 9mm zone of inhibition against staphylococcus aureus. In contrast to gram-positive staphylococcus aureus and gram-negative pseudomonas aeruginosa, Cu MMNPs produce a 12 mm zone of inhibition against gram-negative E. coli and 11 mm zone of inhibition against gram-negative pseudomonas aeruginosa.

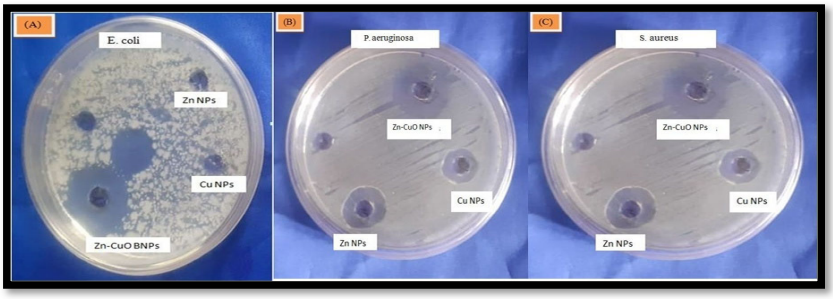

Fig. 8. Antibacterial activity of Borassus flabellifer leaves extract assisted Zn, Cu MMNPs and Zn-Cu BMNPs on (a) Escherichia coli (b) Psuedomonas aeruginosa and (c) Staphylococcus aureus.

Table 4. Inhibition-zone of gram-negative E.coli, gram-negative Pseudomonas aeruginosa, and gram positive Staphylococcus aureus.

Zone of inhibition	E.coli	Psuedomonas aeruginosa	Staphylococcus aureus
Zn MNPs	**12**	**11**	**9**
Cu MNPs	**11**	**12**	**12**
Zn-Cu BMNPs	**25**	**12**	**11**

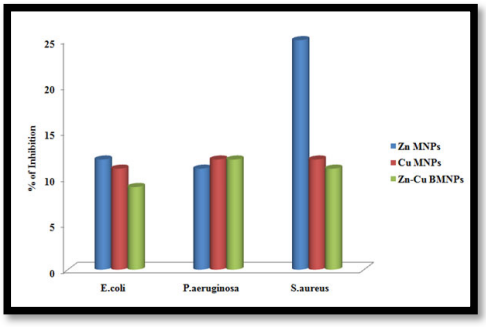

Fig. 9. Antibacterial activity of *Borassus flabellifer* mediated Zn, Cu MNPs and Zn-Cu BMNPs on E.coli, P. aeruginosa, and S. aureus bacterial strains.

3. Conclusion

The use of plant extract for nanoparticle synthesis has several advantages over chemical methods, including environmental friendliness and cohesiveness for pharmaceutical and biomedical applications due to the absence of toxic compounds. Green

synthesis of Borassus flabellifer leaves extract assisted Zn, Cu MMNPs, and Zn-Cu BMNPs has been carried out in the current context. UV-Visible spectroscopy confirmed the formation of Zn, Cu MNPs, and Zn-Cu BMNPs. The crystalline nature of the nanoparticles is confirmed by XRD spectra. HRTEM images determined the approximate particle size of Zn-Cu BMNPs to be 2.2 nm. FESEM images confirm the pseudo spherical and rod shape of Zn-Cu BMNPs. Elemental composition analysis using EDX reveals the presence of Zn, Cu and O. Plant extract serves as a capping and reducing agent in the synthesis of nanoparticles. The antibacterial activity of synthesised nanoparticles against gram-negative E.coli, pseudomonas aeruginosa, and gram-positive staphylococcus aureus bacterial strains was investigated. On these bacterial strains, Zn-Cu BMNPs demonstrated good antibacterial activity. Similarly, Zn-Cu BMNPs have higher antioxidant and anti-diabetic activity than Zn, Cu MNPs. Zn-Cu BMNPs have a higher total phenolic and flavonoid content than Zn, Cu MNPs. Due to the complementary nature of the two metals, bimetallic nanoparticles are more potential.

Acknowledgements

The authors are very thankful to Gurukula Kangri (Deemed to be University), Haridwar, for providing the basic facilities for this research work. The authors are also grateful to Panjab University, Chandigarh, for XRD, FESEM, EDX, HR-TEM and FTIR analysis.

4. Materials and Methods

4.1. Materials

Borassus flabellifer plant (Voucher no: 1/7B 21-12-21) was collected from northern Indian state of Uttar Pradesh and identified by a taxonomist at the Department of Botany, Banaras Hindu University. The chemical Zinc acetate dehydrate $(ZnO_2CCH_3)_2$ $(H_2O)_2$ (98% purity), copper sulphate ($CuSO_4.5H_2O$) used for the analysis was purchased from Merck, Mumbai (India), DPPH, α-amylase, α-glycosidase SRL.Pvt.ld, Mumbai (India). Double distilled water was used as solvent, and also for preparing all the solutions.

4.2. Preparation of extract

The leaves of *Borassus flabellifer* were washed through distilled water to remove dust. The plant samples were dried in the air for 20 days. Then, the leaves were grounded using electrical grinders and then sieved (0.25 mm) to obtain a uniform particle size. Briefly 50g of sample was extracted with 100 ml of water by soxhlet apparatus. The contents were filtered using Whatman filter paper. The extract was used in the synthesis of nanoparticles.

4.3. Preparation of nanoparticles

To synthesize the Zn and Cu NPs, the 50mL *B.flabellifer* leaves extract solution was added drop wise into 200 mL of aqueous solution of 0.5 M Zinc acetate $(ZnO_2CCH_3)_2$ $(H_2O)_2$ and Copper sulphate ($CuSO_4.5H_2O$) (precursor salts) in a separate beakers. But in case of Zn-Cu bimetallic NPs, 50mL B. Flabellifer leaves extract was added into equimolar 200 mL of mixture of zinc acetate $(CH_3COOH)_2$ Zn $2H_2O$ and copper sulphate ($CuSO_4.5H_2O$) (precursor salts). The mixture was kept on the hotplate with stirring at 60 ^{0}C for 1 hour. The color change of the solution (light green to brown) revealed the formation of the NPs. The development of NPs was observed by recording UV-Vis absorption spectra. The formed colloidal solution was centrifuged at 15,000 rpm for 15 min, after this process the solution was washed with distilled water and dried into the oven to obtain the powder form[32]. It is well characterized by using various physico- chemical techniques given below. The flowchart of the method is demonstrated in **Fig. 10.**

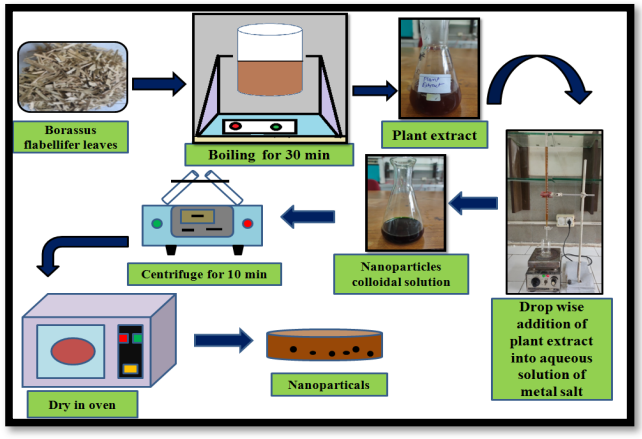

Fig. 10. The flow chart of the synthesis of Zn,Cu MNPs and BMNPs by leaves extract of *Borassus flabellifer.*

4.4. Mechanism Involved In the Growth of NPs

The leaves of *B. flabellifer* were utilised to make Zn, Cu, and Zn-Cu BMNPs using green synthesis. It contains various kinds of phytochemicals, including amine, hydroxyl, alkaloids etc from FT-IR spectra of *Borassus flabellifer* leaves extract **Fig. 11(a).** The GC-MS analysis of the *Borassus flabellifer* plant extract reveals the presence of quinic acid, furaneol, and methyl-2-ethylamino-2-thiazoline, which function as reducing agents and aid in the synthesis of NPs **(Fig. 11(b)). Fig. 12** depicts the general process through which Zn, Cu, and Zn-Cu BMNP samples were prepared. The *Borassus flabellifer* leaves extract and the aqueous solution of the metal precursor were combined in this method. As a result of the mixture, the presence of several phytoconstituents in the *Borassus flabellifer* leaves extract caused the reduction of the metal ions. The role of phytoconstituents in the reduction process a coordination complex is created when the phytoconstituents and metal ions bind together. The intermediate (coordination compound) during the reduction process plays a crucial role in the electron transfer from phytoconstituents to metal. After this cycle is finished, metal oxide NP are created and go through the growth process. The capping agent covers the surface of the nanoparticles and gives them stability after the formation of the metal oxide NPs[33].

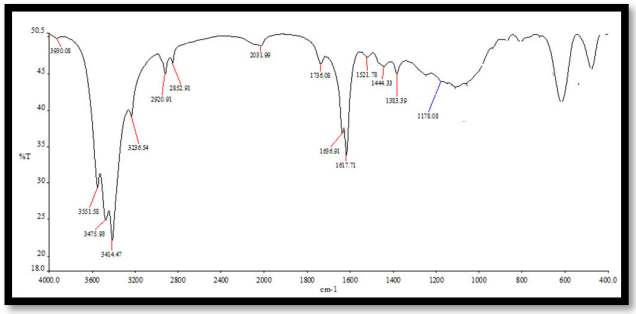

Fig. 11(a). FTIR spectrum of *Borassus flabellifer* leaves extract

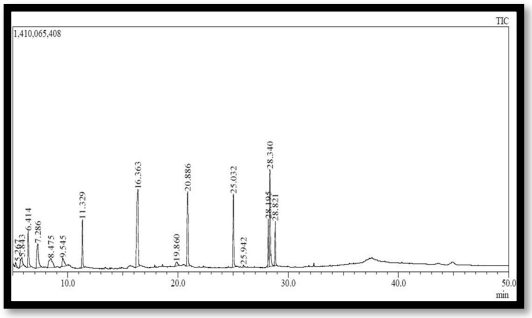

Fig. 11(b). GC-MS chromatogram of *Borassus flabellifer* leaves extract.

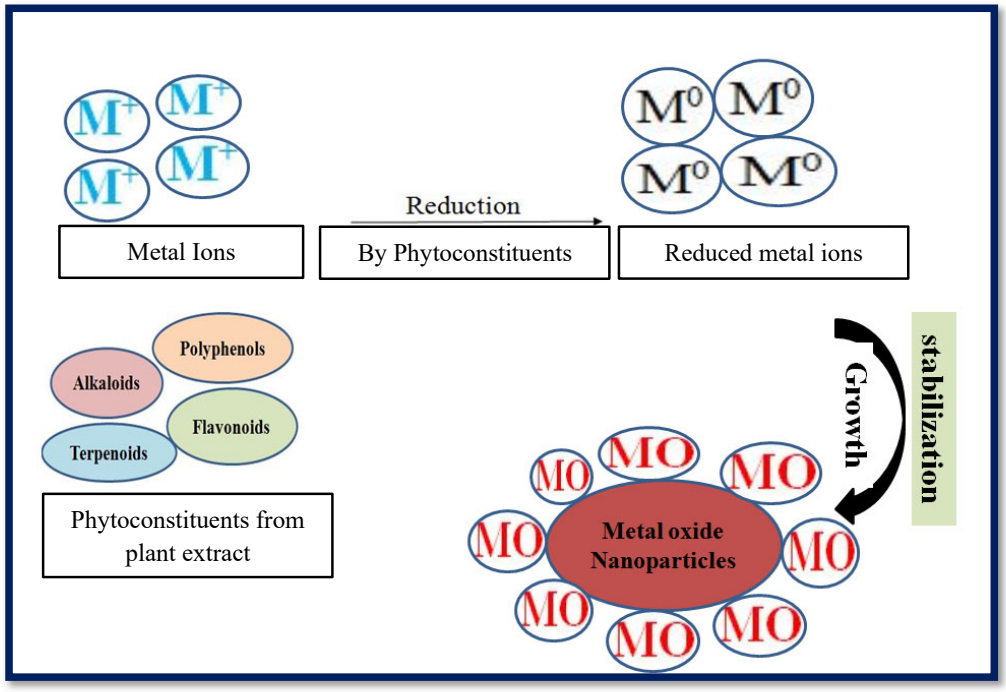

Fig. 12. General mechanism of formation of Zn, Cu MNPs and Zn–Cu BMNPs by leaves extract of *Borassus flabellifer*.

4.5. Characterization of Nanoparticles

The characterization of NPs was done using the following methods: UV-Vis, XRD, FESEM, EDX, and HR-TEM. Systronic double beam spectrophotometer 2203 was used to monitor the reaction. By analysing X-ray diffraction patterns with an X-ray diffractometer that scans at a rate of 2θ angles / min, it was possible to identify the crystalline structure of nanoparticles. Energy dispersive X ray spectroscopy (EDX) was utilised to analyse the elemental composition of metal

nanoparticles, and a field emission electron microscopy (FESEM) (HITACHI SU8010 SERIES) was employed for surface morphological characterisation. High resolution transmission electron microscope (HRTEM) (HRTEM 200 kv JEM 2100F) was used to calculate the particle size.

5. Biological Application

5.1. Estimation of Total Phenolic Content

The total phenolic content was performed by Folin_Ciocalteu Method. 250µl of freshly made Folin-Ciocalteu reagent (sigma Aldrich), 0.75 ml of 20% sodium carbonate (sigma Aldrich), and 3 ml of pure water made up the reaction mixture together with 50µl of each plant extract. The absorbance at 765 nm was measured after 2 hours of reaction at room temperature, and the phenolic content was calculated using gallic acid as a reference[34].

5.2. Estimation of Total Flavonoid Content

Total flavonoid content was carried out using the trichloro aluminium method. 0.1 mL of a 10% (w/v) aluminium chloride solution and 0.1 mL of a 0.1 mM potassium acetate solution were combined with 2.0 mL of the diluted extract or quercetin. For 30 minutes, the mixture was left at room temperature. With the help of a UV-VIS spectrophotometer, the mixture's maximum absorbance was then determined at 415 nm[35].

5.3. Antioxidant Properties

By using DPPH and Phosphomolybdate assay Zn, Cu MNPs and Zn–Cu BMNPs were tested for antioxidant activity.

5.3.1. 1,1-Diphenyl-2-picryl-hydrazyl (DPPH) assay

The radial scavenging activity of the Zn, Cu MNPs and Zn-Cu BMNPs were assessed using DPPH mostly in accordance with Blois's (1958) description with some modifications. Different test tubes were filled with ascorbic acid extracts at various concentrations. MeOH was added to bring the volume to 100 L. These tubes were filled with five millilitres of a 0.1 mM methanol solution of DPPH (sigma Aldrich) and vigorously shaken. For 30 minutes, the tubes were left to stand at 27 ^{0}C. Without any extract, the control was made in the same manner. At 512 nm, the produced samples variations in absorbance were measured[36]. The inhibition % was used to estimate the amount of radical scavenging activity, and the following formula was used to do so:

Radical scavenging activity % = (OD of blank - OD of sample / OD of blank) × 100.

5.3.2. Determination of total antioxidant capacity (Phosphomolybdate assay)

Total antioxidant capacity of samples was estimated by the method reported by Prieto et al. with some modifications[37]. 0.5 ml of samples/standard at different concentrations was mixed with 3 ml of reaction mixture containing 0.6 M sulphuric acid, 28 mM sodium phosphate and 1% ammonium molybdate into the test tubes. The test tubes were incubated at 95°C for 10 minutes to complete the reaction. The absorbance was measured at 695 nm using a spectrophotometer against blank after cooling at RT. Ascorbic acid was used as standard.

5.4. Antidiabetic Activity

By using the α- amylase and α- glucosidase assay, Zn, Cu MNPs and BMNPs were permitted to be tested for antidiabetic activity.

5.4.1. Inhibition assay of α-amylase

The enzymes inhibition procedure of α-amylase was according to the method of Kazeem et al with some modification[38]. The amount of reducing group produced when isolated pancreatic alpha amylase hydrolyzes soluble starch allows for the measurement of α -amylase activity. 3,5-dinitrosalicylic acid is reduced to nitroaminosalicylic acid, which causes a colour shift and a change in the absorbance at 540 nm. **α** - amylase inhibitor that prevents starch hydrolysis reduces absorbance at 540 nm in comparison to the control. As a reference drug for α- amylase Acarbose was used. The half maximum inhibitory concentration was also used to express the percentage (%) of inhibition for α- amylase (IC_{50}). The following is the formula for % inhibition:

$$\% \textbf{ inhibition } = \frac{\textbf{Absorbance of control} - (\textbf{Absorbance of extract})}{\textbf{Absorbance of control}} \times \textbf{100}$$

5.4.2. Inhibition assay of α-glucosidase

The enzymes inhibition procedure of α-glucosidase, was according to the method of Kim et al with slight modification[39]. The enzyme α-glucosidase breaks down the substrate p-nitrophenyl-α-D-glucopyranoside (p-NPG) (SRL Pvt. Ltd.) into p-nitrophenol and D-glucose, respectively, when it is incubated with the substrate. As a reference medication for the assay for α-glucosidase inhibition, acarbose (AC) was utilised. At 410 nm, the emitted p- nitrophenol was measured. Each experiment was run in triplicates with a control set up in parallel without test samples. The half maximal inhibitory concentration was also used to express the percentage of inhibition (%) for all enzymes other than α-glucosidase (IC_{50}). The above formula is for calculating inhibition percentage.

5.5. Antimicrobial Assay

Through the disc diffusion method, an antibacterial experiment was conducted against gramme positive (Staphylococcus aureus) and gramme negative (Escherichia coli and Psuedomonas aeruginosa) pathogens. On sterile filter paper discs that had been infused on the cultured plates, 5 µl of each sample was poured. On separate discs, 5µl of roxithromycin and 5 µl of DMSO were poured as positive and negative controls, respectively. Following a 24-hour incubation period at 370°C, the average diameter of the inhibitory zone was assessed[40].

References

1 Mauricio M. D., Guerra-Ojeda S., Marchio P., Valles S. L., Aldasoro M., Escribano-Lopez I., Herance J. R., Rocha M., Vila J. M., and Victor V. M. **(2018)** Nanoparticles in Medicine: A Focus on Vascular Oxidative Stress. *Oxid. Med. Cell. Longev*., 1–20.

2 Rastogi A., Tripathi D. K., Yadav S., Chauhan D. K., Živˇcák M., Ghorbanpour M., El-Sheery N. I., and Brestic M. **(2019)** Application of Silicon Nanoparticles in Agriculture. *3 Biotech.,* 9 (3) 90.

3 Damian K. C., Roman J. J., Przemysław J. J., and Joanna L. **(2017)** Surface structure of cobalt, palladium, and mixed oxide-based catalysts and their activity in methane combustion studied by means of micro-Raman spectroscopy. *J. Raman Spectrosc.,* 48 (12) 1871-1880.

4 Janaki A. C., Sailatha E., and Gunasekaran S. **(2015)** Synthesis, Characteristics and Antimicrobial Activity of ZnO Nanoparticles. *Spectrochim. Acta A Mol. Biomol. Spectrosc.,* 144 17–22.

5 Kaid M., Ali A., Shamsan A., Younes S., Abdel-Raheem S., Abdul-Malik M., and Salem W. **(2022)** Efficiency of maturation oxidation ponds as a post-treatment technique of wastewater. *Curr. Chem. Lett.,* 11 (4) 415-422.

6 Mohamed S. K., Mague J. T., Akkurt M., Alfayomy A. M., Ragab F. A. F., and Abd Ul-Malik M. A. **(2022)** Crystal structure and Hirshfeld surface analysis of ethyl (3*E*)-5-(4-fluoro-phen-yl)3-{[(4-meth-oxy-phen-yl)formamido]-imino}-7-methyl-2*H*,3*H*,5*H*-[1,3]thia-zolo[3,2-*a*]pyrimidine-6-carboxyl-ate 0.25-hydrate. *Acta Crystallogr E Crystallogr Commun*., 78 (9) 880-884.

7 Ahmeda A. A., Mohamed S. K., and Shaban A. A. **(2022)** Abdel-Raheemd Assessment of the technological quality characters and chemical composition for some Egyptian Faba bean germplasm. *Curr. Chem. Lett.,* 11 359–370.

8 Saleh T. A. **(2020)** Nanomaterials: Classification, Properties, and Environmental Toxicities. *Environ. Technol. Innov.,* 20 1–11.

9 Agarwal H., Venkat Kumar S., and Rajeshkumar S. **(2017)** A Review on Green Synthesis of Zinc Oxide Nanoparticles-An Eco-Friendly Approach. *Resour. Effic. Technol.,* 3 406–413.

10 Thema F. T., Manikandan E., Dhlamini M. S., and Maaza M. **(2015)** Green Synthesis of ZnO Nanoparticles via Agathosma Betulina Natural Extract. *Mater. Lett.,* 161 124–127.

11 Melk M. M., El-Hawary S. S., Melek F. R., Saleh D. O., Ali O. M., Raey M. A., and Selim N. M. **(2021)** Nano Zinc Oxide Green-Synthesized from Plumbago Auriculata Lam. Alcoholic Extract. *Plants.,* 10 2447.

12 Ngoepe N. M., Mbita Z., Mathipa M., Mketo N., Ntsendwana B., and Hintsho-Mbita N. C. **(2018)** Biogenic Synthesis of ZnO Nanoparticles Using Monsonia Burkeana for Use in Photocatalytic, Antibacterial and Anticancer Applications. *Ceram. Int*., 44 16999–17006.

13 Balogun F.O., and Ashafa A. O. T. **(2021)** Potentials of Synthesised Lessertia Montana Zinc Oxide Nanoparticles on Free Radicals-Mediated Oxidative Stress and Carbohydrate- Hydrolysing Enzymes. *Acta Biol. Szeged.,* 64 239–249.

14 Mahlaule-Glory L. M., Mbita Z., Ntsendwana B., Mathipa M. M., Mketo N., and Hintsho-Mbita N. C. **(2019)** ZnO Nanoparticles via Sutherlandia Frutescens Plant Extract: Physical and Biological Properties. *Mater. Res. Express.,* 6 085006.

15 Mbenga Y., Mthiyane M. N., Botha T. L., Horn S., Pieters R., Wepener V., and Onwudiwe D. C. **(2022)** Nanoarchitectonics of ZnO Nanoparticles Mediated by Extract of Tulbaghia Violacea and Their Cytotoxicity Evaluation. *J. Inorg. Organomet. Polym. Mater.,* 32 3249–3259.

16 Diallo A., Ngom B. D., Park E., and Maaza M. **(2015)** Green Synthesis of ZnO Nanoparticles by Aspalathus Linearis: Structural & Optical Properties. *J. Alloy. Compd.*, 646 425–430.

17 Adeyemi J. O., Onwudiwe D. C., and Oyedeji A. O. **(2022)** Biogenic Synthesis of CuO, ZnO, and CuO–ZnO Nanoparticles Using Leaf Extracts of Dovyalis Caffra and Their Biological Properties. *Molecules*., 27 3206.

18 Adeyemi J. O., Elemike E. E., and Onwudiwe D. C. **(2019)** ZnO Nanoparticles Mediated by Aqueous Extracts of Dovyalis Caffra Fruits and the Photocatalytic Evaluations. *Mater. Res. Express.,* 6 1–8.
19 Iravani S. **(2011)** Green Synthesis of Metal Nanoparticles Using Plants. *Green Chem.,* 13 2638–2650.
20 Jodlowski P. J., Chlebda D, Piwowarczyk E, Chrzan M, Jedrzejcczyk R.J. Sitaez M, Wegrzynowicz A, Kolodziej A, and Lojewska J. **(2016)** In situ and operando spectroscopic studies of sonically aided catalysts for biogas exhaust abatement. *J. Mol. Struct*., 11 (26) 132-140.
21 Lojewska J., Knapik A., Jodlowski P., Lojewski T., Kolodziej A. **(2013)** Topography and morphology of multicomponent catalytic materials based on Co, Ce and Pd oxides deposited on metallic structured carriers studied by AFM/Raman interlaced microscopes. *Catal. Today*., 16 11-17.
22 Lwaniszyn M., Piatek M., Gancarczyk A., Jodlowski P. J., Lojewska J., and Kolodziej A. **(2017)** Flow resistance and heat transfer in short channels of metallic monoliths: Experiments versus CFD. *Int. J. Heat Mass Transf.,* 109 778-785.
23 Jodlowski P.J., Damian K. C., Roman J. J., Anna D., Łukasz K., and Maciej S. **(2018)** Characterisation of well-adhered ZrO2 layers produced on structured reactors using the sonochemical sol–gel method. *Appl. Surf. Sci*., 563-574.
24 Chlebda D. K., Stachurska P., Jędrzejczyk R. J., Kuterasiński Ł., Dziedzicka A., Górecka S., Chmielarz L., Łojewska J., Sitarz M., and Jodłowski P. J. **(2018)** $DeNO_x$ Abatement over Sonically Prepared Iron-Substituted Y, USY and MFI Zeolite Catalysts in Lean Exhaust Gas Conditions. *Nanomaterials*., 8 21.
25 Mohammadi R., Aziz A., Yangjeh H., Bayrami A., Latifi S., and Asadollah N. **(2018)** Green Synthesis of ZnO and ZnO / CuO Nanocomposites in Mentha Longifolia Leaf Extract: Characterization and Their Application as Anti-Bacterial Agents. *J. Mater. Sci. Mater. Electron.,* 29 13596–13605.
26 Roy S., and Rhim J. W. **(2019)** Carrageenan-Based Antimicrobial Bionanocomposite Films Incorporated with ZnO Nanoparticles Stabilized by Melanin. *Food Hydrocoll.,* 90 500–507.
27 Gholami P., Dinpazhoh L., Khataee A., and Orooji Y. **(2019)** Sonocatalytic Activity of Biochar-Supported ZnO Nanorods in Degradation of Gemifloxacin: Synergy Study, Effect of Parameters and Phytotoxicity Evaluation. *Ultrason. Sonochem.,* 55 44–56.
28 Dobrucka R. **(2018)** Antioxidant and Catalytic Activity of Biosynthesized CuO Nanoparticles Using Extract of Galeopsidis Herba. *J. Inorg. Organomet*. *Polym. Mater*., 28 812–819.
29 Chang Y.N., Zhang M., Xia L., Zhang J., and Xing G. **(2012)** The Toxic Effects and Mechanisms of CuO and ZnO Nanoparticles. *Materials.,* 5 2850–2871.
30 Shukla A., and Dubey S. **(2022)** A Review: Traditionally Used Medicinal Plants Of Family Arecaceae With Phytoconstituents And Therapeutic Applications. *Int. J. boil. Pharm. Allied sci*., 11 (12) 5864-5877.
31 Sharma G., Kumar A., Sharma S., Naushad M., Dwivedi R. P., Alothman Z. A., and Mola G. T. **(2019)** Novel Development of Nanoparticles to Bimetallic Nanoparticles and Their Composites: A Review. *J. King Saud Univ. Sci.,* 31 257–269.
32 Mohanraj S., Kodhaiyolii S., Rengasamy M., and Pugalenthi V. **(2014)** Green Synthesized Iron Oxide Nanoparticles Effect on Fermentative Hydrogen Production by Clostridium acetobutylicum. *Appl. Biochem. Biotechnol*., 173 318–331.
33 Ezealisiji K. M., Siwe-Noundou X., Maduelosi B., Nwachukwu N., and Krause R. W. M. **(2019)** Green Synthesis of Zinc Oxide Nanoparticles Using Solanum torvum (L) leaf Extract and Evaluation of the Toxicological Profile of the ZnO Nanoparticles–Hydrogel Composite in Wistar Albino Rats. *Int. Nano Lett*., 9 99–107.
34 Zengin G., Uysal S., Ceylan R., and Aktumsek A. (2015) Phenolic constituent, antioxidative and tyrosinase inhibitory activity of Ornithogalum narbonense L. from Turkey: A phytochemical study. *Ind. Crops Prod*., 70 1–6.
35 Pradeep P. M., and Sreerama Y. N. (2015) Impact of processing on the phenolic profiles of small millets: Evaluation of their antioxidant and enzyme inhibitory properties associated with hyperglycemia. *Food Chem.,* 169 455–463.
36 Blois M. S. **(1998)** Antioxidants determination by the use of a stable free radical. *Nature.,* 4617 (181) 1199-1200.
37 Re R., Pellegrini N., Proteggente A., Pannala A. Yang M., and Rice E. C. **(1999)** Antioxidant activity applying an improved ABTS radical cation decolourization assay. *Free Radic. Biol. Med*., 26 1231-1237.
38 Kazeem I. M., and Ashafa T. A. O. **(2015)** In vitro antioxidant and antidiabetic potentials of *Dianthus basuticus* Burtt Davy whole plant extracts. *J. Herb. Med.,* 5 158-164.
39 Kim J. S., Yang J., and Kim M. J. **(2011)** Alpha glucosidase inhibitory effect, anti microbial activity and UPLC analysis of *Rhus verniciflua* under various extract conditions. *J. Med. Plants Res.,* 5 778-783.
40 Arul Ananth D., Sivasudha T., Rameshkumar A., Jeyadevi R., and Aseervatham S. B. **(2013)** Chemical constituents, in vitro antioxidant and antimicrobial potential of Caryota urens L. *Free radic. antioxid.,* 3 107–112.